Direct Measurement of the ^{23}Na$(\alpha,p)^{26}$Mg Reaction Cross Section at Energies Relevant for the Production of Galactic ^{26}Al

S. Almaraz-Calderon,[1,*] P. F. Bertone,[1,†] M. Alcorta,[1,‡] M. Albers,[1] C. M. Deibel,[2] C. R. Hoffman,[1] C. L. Jiang,[1] S. T. Marley,[1,§] K. E. Rehm,[1] and C. Ugalde[1,3]

[1]*Physics Division, Argonne National Laboratory, Argonne, Illinois 60439, USA*

[2]*Department of Physics and Astronomy, Louisiana State University, Baton Rouge, Louisiana 70803, USA*

[3]*Department of Astronomy and Astrophysics, University of Chicago, Chicago, Illinois 60637, USA*

(Received 25 November 2013; revised manuscript received 20 January 2014; published 17 April 2014)

The 1809-keV γ ray from the decay of ^{26}Al^g is an important target for γ-ray astronomy. In the convective C/Ne burning shell of massive presupernova stars, the ^{23}Na$(\alpha, p)^{26}$Mg reaction directly influences the production of ^{26}Al. We have performed a direct measurement of the ^{23}Na$(\alpha, p)^{26}$Mg reaction cross section at the appropriate astrophysically important energies. The stellar rate calculated in the present work is larger than the recommended rate by nearly a factor of 40 and could strongly affect the production of ^{26}Al in massive stars.

DOI: 10.1103/PhysRevLett.112.152701 PACS numbers: 25.60.Dz, 26.30.-k, 26.50.+x, 27.30.+t

The observation of ^{26}Al in the galactic interstellar medium via its emission line at 1809 keV confirmed that active nucleosynthesis is occurring in the Galaxy [1]. It also provides strong constraints to stellar and supernova nucleosynthesis models. It is therefore of fundamental importance to understand all mechanisms that synthesize or destroy ^{26}Al in astrophysical environments.

The origin of ^{26}Al remains controversial, although the observational evidence favors massive stars as a source [2]. The irregular distribution of ^{26}Al emission seen along the plane of the Galaxy provided the main argument for the idea that massive stars dominate the production of ^{26}Al [3]. Massive stars may produce ^{26}Al during several different phases of their evolution: during presupernova stages in C/Ne convective shell burning, during core collapse via Ne/C burning, and during convective core H burning for stars with $M \geq 30\ M_\odot$.

In the C/Ne convective shell of a presupernova star ($T \sim 1.25$ GK) the production of ^{26}Al is dominated by the ^{25}Mg$(p,\gamma)^{26}$Al reaction, where ^{25}Mg is created by the ^{22}Ne$(\alpha,n)^{25}$Mg and ^{24}Mg$(n,\gamma)^{25}$Mg reactions. The charged particles driving these mechanisms come primarily from the C burning reactions ^{12}C$(^{12}$C$, p)^{23}$Ne and ^{12}C$(^{12}$C$, \alpha)^{20}$Ne. However, a recent detailed sensitivity study of ^{26}Al production in massive stars found that the second most important source of protons is the ^{23}Na$(\alpha, p)^{26}$Mg reaction [2]. Using temperature-density-time profiles from state-of-the-art stellar models [4], the authors performed postprocessing calculations, varying 1648 nuclear reactions in a network connecting 175 nuclides from H to Ca, and tracked the resulting changes in the final ^{26}Al abundances. They found that a factor of 10 increase in the ^{23}Na$(\alpha, p)^{26}$Mg reaction rate would result in a factor of 3 change in the ^{26}Al abundance, therefore concluding that the ^{23}Na$(\alpha, p)^{26}$Mg reaction should be a high-priority target for future measurements [2].

Earlier experiments of the ^{23}Na$(\alpha, p)^{26}$Mg reaction ([5,6]) suffered from the instability of the NaCl targets (see Refs. [7,8]). Following the experiment by Kuperus [5], studying the ground state transition in ^{26}Mg, Whitmire and Davids reported a direct measurement of the ground and first excited states in ^{26}Mg [6]. All these attempts to measure absolute resonance strengths were severely compromised by the instability of the target since sodium targets evaporate quickly and change their stoichiometry under beam bombardment [7,8], making absolute measurements nearly impossible. Because of the substantial uncertainties involved in the analysis of Ref. [6], the authors of Ref. [2] preferred to use an estimate for the ^{23}Na$(\alpha, p)^{26}$Mg reaction rate provided by a statistical model [9]. Depending on the choice of optical model potential and level density parametrization, statistical models can be uncertain by a factor of 2 [10]. The case of the ^{23}Na$(\alpha, p)^{26}$Mg reaction is potentially even more uncertain due to the low level density at the relevant energies.

In this Letter, we report on the results of a direct measurement of the ^{23}Na$(\alpha, p)^{26}$Mg reaction cross section. The present experiment was carried out in inverse kinematics, i.e., bombarding a He gas target with a ^{23}Na beam, which avoids the uncertainties due to target deterioration suffered by the previous measurements [5,6]. Constraints on angle-integrated cross sections for the reactions ^{23}Na$(\alpha, p_0)^{26}$Mg and ^{23}Na$(\alpha, p_1)^{26}$Mg* have been extracted in the energy range of $E_{\text{c.m.}} = 1.3$ to 2.5 MeV. Our measurements include astrophysically relevant energies for the production of ^{26}Al in massive stars. The corresponding stellar reaction rate has been recalculated and compared with the current recommended rate,

which is based on a statistical model calculation [2]. The rate calculated in this work is consistently larger than the recommended rate by factor of ~40, which is substantially bigger than the increase needed to generate a factor of 3 change in the ^{26}Al abundance.

The measurement of the ^{23}Na$(\alpha, p)^{26}$Mg reaction cross section was performed using a ^{23}Na beam from the Argonne ATLAS accelerator to bombard a cryogenic ^{4}He gas target. The target cell was 1.5 mm in length and was kept at liquid nitrogen temperatures [11]. Under these conditions, 550 Torr of ^{4}He at 90 K yielded an effective ^{4}He target thickness of $\sim 59\ \mu g/cm^2$. The temperature and pressure of the gas was constantly monitored during the experiment. The gas target system used $1.40(5)\ mg/cm^2$ thick titanium foils as windows to minimize the energy loss while allowing for high gas pressures. The thickness of the titanium windows was independently determined by the energy loss technique, placing them in front of a split-pole spectrograph, and by the kinematics of the detected protons.

Four ^{23}Na beam energies of 30, 28, 26, and 23 MeV were used in this experiment with typical intensities of 2×10^8 pps. A schematic of the experimental setup is shown in Fig. 1. An annular 500-μm thick silicon strip detector was used to identify the protons from the reaction. It was placed 20 cm downstream from the target, covering an angular range of $\theta_{lab} = 6.8°$ to 13.5°. An aluminum foil 70-μm thick (40 μm for the lowest energy point) was used to ensure that only protons from the ground state and first excited state of ^{26}Mg reach the detector with acceptable energy losses while blocking the elastically scattered ^{23}Na beam and recoil α particles. At these energies, no other light-particle reaction channels are energetically allowed. Therefore, the predominant sources of background are knock-out protons from hydrogen in the Ti windows of the gas target. Background measurements with an empty gas target under identical conditions were taken at each beam energy. In order to monitor the beam intensity, a 120 $\mu g/cm^2$ thick Au foil mounted on a 10 $\mu g/cm^2$ thick natural C backing was placed 3.9 cm upstream of the target. Beam particles that underwent Rutherford scattering were measured with an annular 300-μm thick silicon strip detector placed 3.8 cm upstream from the Au foil.

The computer codes SRIM [12] and LISE [13] were used to calculate the energy loss of the ions in the foils and target

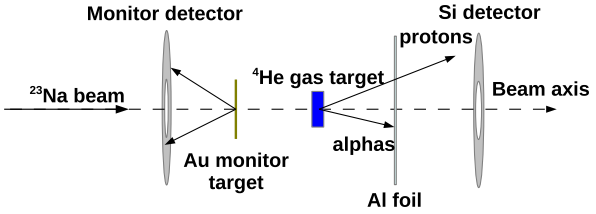

FIG. 1 (color online). Schematic view of the experimental setup.

as well as the response of the silicon detectors. The main energy loss was due to the titanium windows of the ^{4}He gas cell. The energy spread of the beam after the titanium foil at the entrance of the gas target was below 100 keV for all beam energies. The distance between the He gas target and the detector was chosen as a compromise between detection efficiency and energy resolution for protons passing through the titanium exit window and the aluminum foil mounted in front of the Si detector. Smaller distances would create larger emission angles for the protons leading to a much larger energy spread. The experimental data were found to be in very good agreement with simulations at all energies.

After passing through the Au target and the entrance window of the gas target, the ^{23}Na beam covered the center-of-mass energy ranges 2.50–2.33, 2.18–2.02, 1.87–1.70, and 1.42–1.26 MeV, as determined by the energy loss on the 59 $\mu g/cm^2$ ^{4}He target for the four beam energies used.

The number of incident particles was calculated from the yield of Rutherford scattered ^{23}Na ions from the Au foil impinging on the monitor detector. By comparing the number of beam particles taken with and without gas in the cell, a normalization factor for each energy was extracted and used to subtract the background contribution from the Ti windows.

The proton spectra obtained in the experiment are shown in Fig. 2. The differential cross sections for the ^{23}Na$(\alpha, p_0)^{26}$Mg and ^{23}Na$(\alpha, p_1)^{26}$Mg* reactions could be extracted for the two highest beam energies (30 and 28 MeV). For the 26 MeV beam energy, only the p_0 channel was measured since protons from the p_1 state overlapped with the background protons from the Ti windows. For the lowest energy measurement at 23 MeV, only an upper limit for p_0 can be quoted.

Because of the effect of the extended gas target, our measurement averages the cross section in the corresponding energy intervals given above. Since the cross section increases with energy, it is expected that most of the proton yield will come from the beginning of the target, where the energy of the beam is higher, rather than from the end of the target where the energy of the beam has decreased. We used the cross sections predicted by the Hauser-Feshbach (HF) code CIGAR [14] to calculate a weighted average energy ($\langle E \rangle_W$) for each energy interval. The resulting effect is almost negligible for the two highest energies. It is appreciable for the two lowest beam energies, moving the average about ~20 keV towards the high end of the corresponding energy interval.

The geometry of the cryogenic gas target allowed only a measurement of the differential cross section in the c.m. region of $\theta_{c.m.} = 161°$ to 171°. To extract the angular distributions, the rings of the silicon detector were combined in four groups of four rings. An example of the measured angular distributions is shown in Fig. 3. The angle-integrated cross sections were obtained by

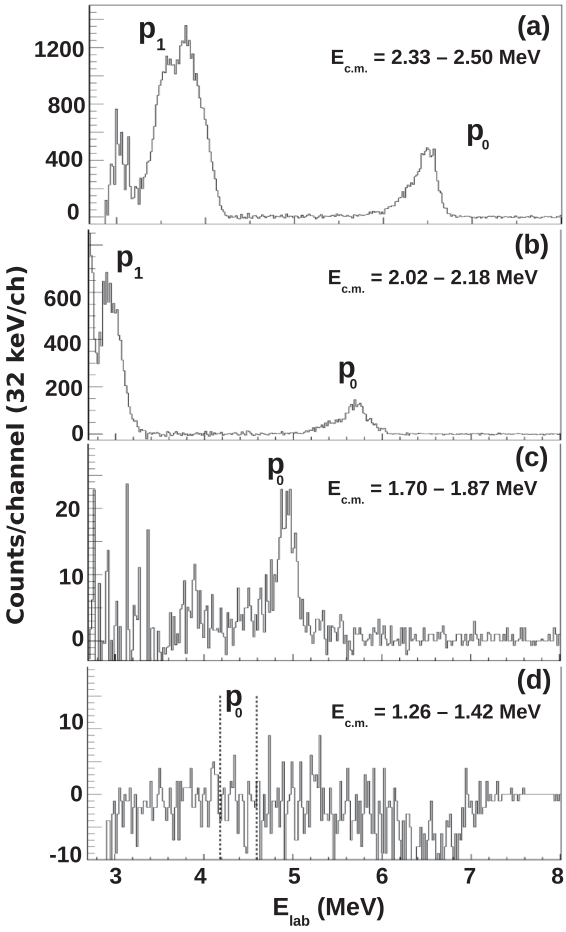

FIG. 2. Proton spectra measured for the ^{23}Na(α, p) reaction at the four beam energies. The background from the titanium windows was subtracted using a scaling factor from the back-scattered monitor detector (see text for details). For the highest two energies, the p_0 and p_1 reaction channels are clearly visible. For 26 MeV (c), only the p_0 channel is observed, while for the lowest beam energy, only an upper limit for the p_0 channel was extracted, the expected position of the p_0 peak is shown by the dashed lines.

multiplying the differential cross sections by $\sin\theta$ and using the average values for the integration. Measurements of complete angular distributions in the neighboring system ^{27}Al$(\alpha, p)^{30}$Si populating the ground state and first two states in ^{30}Si have been performed in Refs. [15,16]. The angular momentum transfers are similar in the two cases with an unpaired $l = 2$ proton ($d_{3/2}$ for ^{23}Na and $d_{5/2}$ for ^{27}Al) and for energies below 3.5 MeV/u are found to be symmetric around 90° following a representation of the experimental data by Legendre polynomials. We have used the parameters obtained in Ref. [15] and normalized the distribution to the measured differential cross sections at $\theta_{\text{c.m.}} = 161°$ to 171°. Integrating the distribution in the full angular range gave integrated cross sections which are tabulated in Table I. We have given a conservative 50% uncertainty to these values.

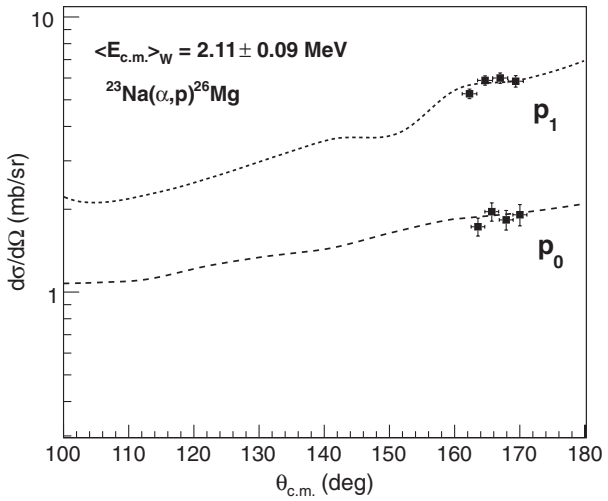

FIG. 3. Example of the angular distribution of the ^{23}Na$(\alpha, p_0)^{26}$Mg and ^{23}Na$(\alpha, p_1)^{26}$Mg* cross sections measured in the present work. The lines indicate the angular distributions measured for the equivalent states in the ^{27}Al$(\alpha, p)^{30}$Si reaction from Ref. [15].

From Figs. 2 and 3 it is observed that the cross section corresponding to the p_1 channel is substantially higher than the one corresponding to the p_0 channel, in agreement with the results obtained for ^{27}Al$(\alpha, p)^{30}$Si. The spin-parity of the nuclei involved as well as the angular momentum transfers, favor the p_1 reaction channel over p_0, which is in agreement with our current measurement. The second excited state in ^{26}Mg has the same spin-parity as the first one (2^+). It is, however, more than 1 MeV higher in excitation energy (2.938 MeV), and for this reason it is not included in the calculation of the reaction rate. A HF calculation indicates that at the highest energy measured in the present work (2.42 MeV), the p_2 component would make a contribution of about 6% with respect to the p_1 component. At lower energies this contribution becomes negligible.

A comparison of the measured cross sections with the predictions by the Hauser-Feshbach statistical model codes CIGAR [14] and TALYS [17] is presented in Fig. 4. The HF calculations agree with each other within a factor of 2, with the larger differences found at energies above 2 MeV.

TABLE I. Cross sections for the ^{23}Na$(\alpha, p)^{26}$Mg reaction obtained at each ^{23}Na beam energy.

E_{beam} (MeV)	$\langle E_{\text{c.m.}}\rangle_W$ (MeV)	$\sigma(\alpha, p_0)$ (mb)	$\sigma(\alpha, p_1)$ (mb)	$\sigma(\alpha, p)$ (mb)
30	2.42 ± 0.09	25 ± 12	100 ± 50	125 ± 63
28	2.11 ± 0.09	8 ± 4	26 ± 13	34 ± 17
26	1.81 ± 0.11	1.2 ± 0.7	3[a]	4.2[a]
23	1.36 ± 0.10	≤ 0.18	≤ 0.27[a]	≤ 0.45[a]

[a]Extrapolated from the fit of the CIGAR calculation to the experimental data.

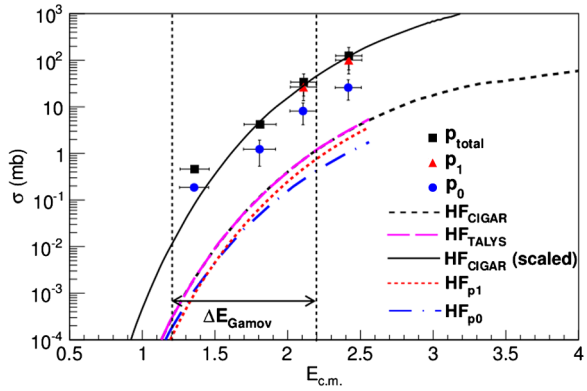

FIG. 4 (color online). Cross section for the ^{23}Na$(\alpha, p)^{26}$Mg reaction. The lines corresponds to HF calculations performed with the codes CIGAR [14] and TALYS [17]. The solid line is the CIGAR calculation multiplied by a factor of 38 to fit the experimental data. The Gamov window for $T = 1.25$ GK is indicated by the vertical lines.

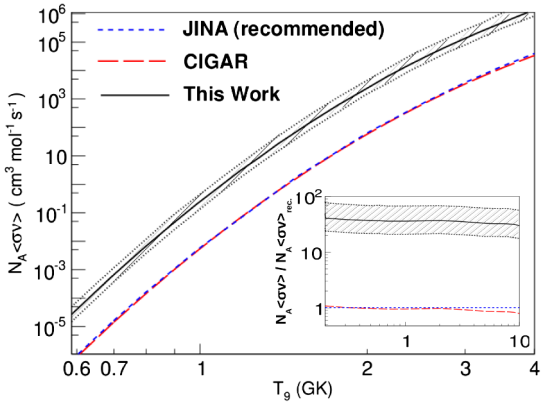

FIG. 5 (color online). The ^{23}Na$(\alpha, p)^{26}$Mg reaction rate calculated in the present work using CINA [18]. The dotted black lines indicate the error band (dashed area). The recommended reaction rate [19] as well as the CIGAR rate [14] are shown for comparison. The ratios of the different rates to the recommended rate are shown in the inset.

While the energy dependence of the cross section is in agreement with the statistical model calculations, the magnitude of the theoretical predictions are considerably smaller. A scaling factor of 9 in the total cross section is needed to fit the p_0 channel while a factor of 29 is needed to fit the p_1 channel. In total, the extrapolated cross sections are found to be a factor of 38 higher compared to the CIGAR calculations. A summary of the results obtained in the present work is given in Table I. The cross section of the (α, p_1) channel for the two lowest energy points was calculated by extrapolating the fit of the CIGAR calculation to the experimental data at the two higher energies. Based on the information on the resonance structure from previous measurements [5,6] we found that the 200 keV average in the experimental energy provides a meaningful average cross section given the current experimental uncertainties.

The astrophysical reaction rate was calculated using the Oak Ridge Computational Infrastructure for Nuclear Astrophysics (CINA) [18] and is shown in Fig. 5 compared with the CIGAR rate [14], as well as with the recommended rate [9] taken from the JINA REACTLIB database [19]. While the statistical model rates are in very good agreement with each other, the rate calculated on the basis of the present experimental work is consistently larger by approximately a factor of ~40. An error band was extracted by varying the rate to fit the upper and lower ends of the experimental error bars, resulting in scaling factors of 65 and 22, respectively. The reaction rate presented in this work can be parametrized by the analytic function

$$N_A\langle\sigma\nu\rangle = \exp\left[a_0 + \frac{a_1}{T_9} + \frac{a_2}{T_9^{1/3}} + a_3 T_9^{1/3} + a_4 T_9 + a_5 T_9^{5/3} + a_6 \ln(T_9)\right], \quad (1)$$

where the constants were found to be $a_0 = 52.6084$, $a_1 = -0.7355$, $a_2 = -22.3367$, $a_3 = -31.2889$, $a_4 = 0.1379$, $a_5 = 0.0518$, and $a_6 = 17.5418$ [18].

In summary, by measuring the ^{23}Na$(\alpha, p)^{26}$Mg reaction cross section at astrophysically relevant energies, we have found a considerable increase of the reaction rate with respect to the recommended rate which is based on statistical models. Specifically, at $T \sim 1.25$ GK where the ^{23}Na$(\alpha, p)^{26}$Mg reaction rate is the second most important source of protons for production of ^{26}Al in massive stars, the increase in the reaction rate as calculated in the present work, is expected to have a strong effect in the abundance of ^{26}Al in this astrophysical scenario, since our result is significantly larger than the factor of 10 increase in the reaction rate needed to change the abundance of ^{26}Al by a factor of 3 [2].

This work is supported by the U.S. DOE Office of Nuclear Physics under Contract No. DE-AC02-06CH11357.

*salmaraz@phy.anl.gov
†Present address: Marshall Space Flight Center, Huntsville, Alabama 35811, USA.
peter.bertone@nasa.gov
‡Present address: TRIUMF, Vancouver, British Columbia V6T 2A3, Canada.
§Present address: Department of Physics, University of Notre Dame, Notre Dame, Indiana 46556, USA.

[1] W. Mahoney, J. Ling, A. Jacobson, and R. Lingenfelte, Astrophys. J. **262**, 742 (1982).
[2] C. Iliadis, A. Champagne, A. Chieffi, and M. Limongi, Astrophys. J. **193**, 16 (2011).
[3] R. Diehl *et al.*, Nature (London) **439**, 45 (2006).
[4] M. Limongi and A. Chieffi, Astrophys. J. **647**, 483 (2006).

[5] J. Kuperus, Physica (Amsterdam) **30**, 2253 (1964).
[6] D. P. Whitmire, and C. N. Davids, Phys. Rev. C **9**, 996 (1974), and references therein.
[7] B. M. Paine, S. R. Kennett, and D. G. Sargood, Phys. Rev. C **17**, 1550 (1978).
[8] C. Rowland, C. Iliadis, A. E. Champagne, and J. Mosher, Phys. Rev. C **65**, 064609 (2002).
[9] T. Rauscher and F.-K. Thielemann, At. Data Nucl. Data Tables **75**, 1 (2000).
[10] B. M. Oginni, C. Iliadis, and A. E. Champagne, Phys. Rev. C **83**, 025802 (2011).
[11] K. E. Rehm, J. P. Greene, B. Harss, D. Henderson, C. L. Jiang, R. C. Pardo, B. Zabransky, and M. Paul, Nucl. Instrum. Methods Phys. Res., Sect. A **647**, 3 (2011).
[12] J. F. Ziegler, Nucl. Instrum. Methods Phys. Res., Sect. B **219–220**, 1027 (2004).
[13] O. Tarasov and D. Bazin, Nucl. Instrum. Methods Phys. Res., Sect. B **266**, 4657 (2008).
[14] R. Crowter, Masters thesis, University of Surrey, 2007.
[15] A. V. Spasskii, I. B. Teplov, and L. N. Fateeva, Sov. J. Nucl. Phys. **7**, 175 (1968).
[16] F. de S. Barros, P. D. Forsyth, A. A. Jaffe, and I. J. Taylor, Proc. Phys. Soc. **73**, 793 (1959).
[17] A. J. Koning, S. Hilaire, and M. C. Duijvestijn, TALYS-1.0, *Proceedings of the International Conference on Nuclear Data for Science and Technology, 2007, Nice, France*, edited by O. Bersillon, F. Gunsing, E. Bauge, R. Jacqmin, and S. Leray (EDP Sciences, Les Ulis, France, 2008), p. 211.
[18] The Computational Infrastructure for Nuclear Astrophysics (CINA). www.nucastrodata.org.
[19] R. H. Cyburt *et al.*, Astrophys. J. Suppl. Ser. **189**, 240 (2010).